Clin Neuroradiol (2019) 29:51–64
https://doi.org/10.1007/s00062-017-0654-0

ORIGINAL ARTICLE

Cortical and Subcortical Morphometric and Iron Changes in Relapsing-Remitting Multiple Sclerosis and Their Association with White Matter T2 Lesion Load

A 3-Tesla Magnetic Resonance Imaging Study

Ali Al-Radaideh[1] · Imad Athamneh[2] · Hadeel Alabadi[2] · Majed Hbahbih[3]

Received: 14 October 2017 / Accepted: 8 December 2017 / Published online: 3 January 2018

Abstract

Introduction This study was carried out to investigate the global and regional morphometric and iron changes in grey matter (GM) of multiple sclerosis (MS) patients and link them to the white matter (WM) lesions in a multimodal magnetic resonance imaging approach.

Material and Methods The study involved 30 relapsing-remitting MS (RRMS) patients along with 30 age-matched healthy controls (HC) who were scanned on a 3T Siemens Trio system. The scanning protocol included a 3D, high resolution T1, T2, and T2*-weighted sequences. The T1-w images were used in FreeSurfer for cortical reconstruction and volumetric segmentation, while T2-w images were used to extract the WM T2 lesions; however, iron and magnetic susceptibility were calculated from the phase data of the T2*-w sequence. Surface-based analyses were performed in FreeSurfer to investigate the regional cortical morphometric changes and their correlations with the expanded disability status scale (EDSS), WM T2 lesions load, cortical iron deposition and magnetic susceptibility.

Results Significant differences were detected between the RRMS patients and HC for all cortical and subcortical morphometric changes. The EDSS and T2 lesion load showed weak to moderate correlation with the reduced cortical morphometric measurements, increased cortical magnetic susceptibility and iron concentration. All deep grey matter (dGM) volumes showed a significant strong positive correlation with the cortical surface area and volume in RRMS patients and HC.

Conclusions Grey matter is very much involved in the RRMS and cortical morphometric changes occur in a non-uniform pattern and are very likely to be associated with cortical iron deposition and magnetic susceptibility, dGM atrophy, WM T2 lesion load, and disability.

Keywords Relapsing-remitting multiple sclerosis · Cortical grey matter · Magnetic susceptibility mapping · Iron · Lesion load

Electronic supplementary material The online version of this article (https://doi.org/10.1007/s00062-017-0654-0) contains supplementary material, which is available to authorized users.

✉ Ali Al-Radaideh
ali.radaideh@hu.edu.jo

Imad Athamneh
imadathamneh@gmail.com

Hadeel Alabadi
hadeelshehab3@gmail.com

Majed Hbahbih
majed_hab@yahoo.co.uk

[1] Departmentof Medical Imaging, Faculty of Allied Health Sciences, The Hashemite University, Zarqa, Jordan

[2] Department of Radiology, King Hussien Medical Center, Jordanian Royal Medical Services, Amman, Jordan

[3] Department of Internal Medicine, Neurology, King Hussein Medical Centre, Jordanian Royal Medical Services, Amman, Jordan

Introduction

Multiple sclerosis (MS) is an autoimmune disease affecting the central nervous system (CNS), and appears as acute focal inflammatory demyelination and axonal loss with limited remyelination, gliosis, and atrophy, and it is manifested as chronic multifocal sclerotic plaques [1]. Most MS patients begin with a relapsing-remitting (RRMS) course, with the majority developing a secondary progressive MS (SPMS) with irreversible disabilities. Conventional magnetic resonance imaging (MRI) measurements have uncovered remarkable spatial and temporal information and established a framework for the clinical diagnosis and management of MS. These measures include CNS atrophy and lesions (T2 hyperintense, T1 hypointense, and gadolinium enhancement); however, these measures lack the specificity for the occult (diffuse) disease in normal appearing brain tissue and thus show a weak correlation with clinical status of MS patients [2, 3]. The latter instigated the development of new quantitative MRI techniques, such as diffusion tensor imaging (DTI), magnetic resonance spectroscopy (MRS), relaxometry, phase and magnetic susceptibility imaging. Although MS is typically considered as a white matter (WM) disease due to the more readily detected lesions in the white matter by histopathology and MRI, the involvement of the cortical and deep grey matter (GM) in the development of the disease has been confirmed by different pathological studies [4–8]. Damage has frequently been observed in the cortical grey matter, which can further explain the physical and cognitive decline in patients with multiple sclerosis better than white matter abnormalities [9–11]. Grey matter lesions and grey matter atrophy are presumed to reflect different but interrelated pathological processes. Grey matter lesions are characterized by inflammatory demyelination and represent the initial phase of grey matter atrophy. The latter reflects a combination of demyelination, neurite transection [12], and reduced synapse or glial densities [13, 14]. Furthermore, grey matter atrophy largely contributes to the whole brain atrophy in patients suffering from MS [15, 16]. Accumulation of brain iron has been suggested as a biomarker of neurodegeneration and is considered as one of the most important inducers of oxidative stress in the brain [17, 18]. The oxidative damage produced by iron has been implicated in the injury of oligodendrocytes and myelin in MS [19]; therefore, the amount of iron deposition could reflect the extent of tissue damage. There is growing evidence of iron accumulation in the deep grey matter of patients with multiple sclerosis (MS), from both postmortem and imaging studies of healthy individuals and those with neurodegenerative diseases, and it was found to occur in the earliest stages of the MS disease [20]; however, increased cortical iron deposition has only been seen in postmortem studies of neurodegenerative diseases and healthy aging [21–24]. Accurate measurement of cortical iron accumulation in vivo in MS patients is still one of the main challenges due to the diminutive thickness of the cortex and its relatively low iron content [25]; however, an in vivo assessment of the iron content of the cerebral cortex was performed in a group of healthy aging volunteers using the phase images of T2*-weighted images at ultra-high field MRI (7 T; [25]). Accurate assessment of cortical iron accumulation could become a novel biomarker for the onset and progression of multiple sclerosis and other neurodegenerative diseases. White matter lesion load measurements, on the other hand, have shown generally unreliable associations with clinical disability in MS urging the use of composite MRI measurements to link MRI with clinical information. Combined information on lesions and atrophy can provide improved longitudinal correlations with physical disability [24] and MS phenotypes [26]; however, white matter lesion load has been reported to be the most relevant predictor of the iron deposition in deep grey matter structures [27].

The aim of the present study was to investigate the global and regional morphometric (thickness, surface area, and volume) changes and iron accumulation in the cortical and subcortical grey matter structures and T2 lesion loads in the white matter of a group of RRMS patients and their possible associations by utilizing a combined and multimodal approach of different quantitative MRI indices.

Materials and Methods

Study Population

A total of 30 patients with RRMS (17 females, 13 males; mean age 31.27 years; age range 20–53 years) were recruited from the neurology clinic at the Royal Medical Services (RMS) along with 30 age-matched healthy controls (16 females, 14 males; mean age 32.35 years; age range 20–54 years). Table 1 summarizes the characteristics of the two study groups. The present study was approved by the RMS ethics committee and carried out in accordance with The Code of Ethics of the World Medical Association (Declaration of Helsinki). All participants were asked to sign a consent form and fill out the MRI safety questionnaire before participating in the study. Neurological examinations were carried out by a consultant neurologist who was qualified to perform the expanded disability status scale (EDSS) assessments according to the standardized scoring system in Neurostatus (http://www.neurostatus.net/scoring/index.php). A functional system (FS) grade was obtained for each area representing a different function of the central nervous system (pyramidal, brain stem, visual, cerebellar, sensory, bowel and bladder, and higher cerebral). The

Table 1 Characteristics of study controls and relapsing remitting multiple sclerosis (RRMS) patients

Subjects	RRMS	Controls
Number	30	30
Sex (male/female)	13/17	14/16
Age range (years)	20–53	20–54
Mean age ± SD (years)	31.27 ± 10.2	32.35 ± 8.7
EDSS range	0–6.5	–
Mean EDSS ± SD	2.67 ± 2.19	–
Time since diagnosis range (months)	1–179	–
Mean time since diagnosis ± SD (months)	46.03 ± 14.10	–
Number of relapses (range)	1–8	–
Mean number of relapses	2.9 ± 1.42	–

SD standard deviation, *EDSS* expanded disability status scale

FS scores reflected the degree of disability across all these areas, as found on the neurological assessment. The final EDSS score was calculated on the basis of the combined/summarized FS scores, giving a value of between 0 (normal examination) and 10 (death due to MS).

Magnetic Resonance Imaging (MRI) Acquisition

Scanning was performed on a 3T Siemens Trio MRI (Siemens Healthcare, Erlangen, Germany) system. The imaging protocol included the following imaging sequences: high resolution 3D-T1 weighted magnetization prepared-rapid acquisition gradient echo (MPRAGE) with 0.9 mm^3 isotropic spatial resolution; reconstruction matrix = 224 × 256; TE = 3.4 ms; TR = 1900 ms; inversion time = 900 ms; flip angle = 9°; scan time = 5:53 min. High resolution 3D-T2* weighted gradient echo sequence with 1 mm^3 isotropic spatial resolution, reconstruction matrix = 256 × 256; TE = 20 ms; TR = 33 ms; flip angle = 15°; scan time = 5:30 min. Both magnitude and phase images were reconstructed for further analysis. The 3D-T2 weighted fluid attenuated inversion recovery (FLAIR) with 1 mm^3 isotropic spatial resolution; reconstruction matrix = 256 × 256; TE = 390 ms; TR = 5000 ms; flip angle = 90°; scan time = 5:52 min.

Image Post-Processing and Analysis

Magnetic Susceptibility Mapping and Iron Calculations

Magnetic susceptibility mapping was performed as described in a previous publication [20]. In summary, the T2* weighted magnitude (Fig. 1a) and its corresponding phase (Fig. 1b) images of each subject were first spatially co-registered to the high resolution, T1 MPRAGE (Fig. 1g). The co-registered magnitude and phase images were then merged into a single volume. From the magnitude data, a binary mask of the brain was produced in FSL (www.fmrib.ox.ac.uk/fsl/) and this was applied to the phase data. Prelude in FMRIB software library (FSL) was used to unwrap the resulting phase images within the mask (Fig. 1c). These phase data were then high-pass filtered to remove the effects of large-scale background fields, such as those near the air/tissue boundaries at the sinuses. This was achieved using a dipole fitting method [28]. After filtering, the phase data were divided by $\gamma B_0 TE$ to yield field-shift maps. Susceptibility maps (Fig. 1d) were then created from these filtered field maps, using a threshold-based method [28].

The phase values of cerebrospinal fluid (CSF) were used as a reference for iron calculation because it is assumed that CSF contains a negligible amount of MR-visible iron [29]. The phase differences relative to that of the CSF were converted to iron concentration according to the equation proposed by Haacke: 0.276 radians of the phase difference to be equivalent to 240 μg Fe/g tissue [30].

White Matter T2 Lesion Load Calculation

For each patient white matter T2-hyperintense lesion volume measurements were obtained using a semi-automated segmentation technique based on the fuzzy connectedness algorithm [31] in Jim software (Jim version 7; Xinapse Systems, Essex, England). The T2-weighted FLAIR images were spatially co-registered to the high-resolution, T1-weighted MPRAGE images using rigid body registration with six degrees of freedom in Jim software in order to make the two volumes dimensionally similar. As part of image co-registration process, T2-FLAIR and T1-MPRAGE images were first corrected for signal intensity non-uniformity (bias field). The registered T2-FLAIR images were used to define "seed" points in the center of each MS lesion and save them for each patient. Thereafter, T1 and T2-weighted images, "seed" points, and the lesion prior probability template image, which was constructed from a large sample of MS patient scans and implemented into the Jim software, were loaded and used by the "MS Finder" tool in Jim to find the MS lesions based on the fuzzy connectedness algorithm [31]. The total lesion volume was then calculated

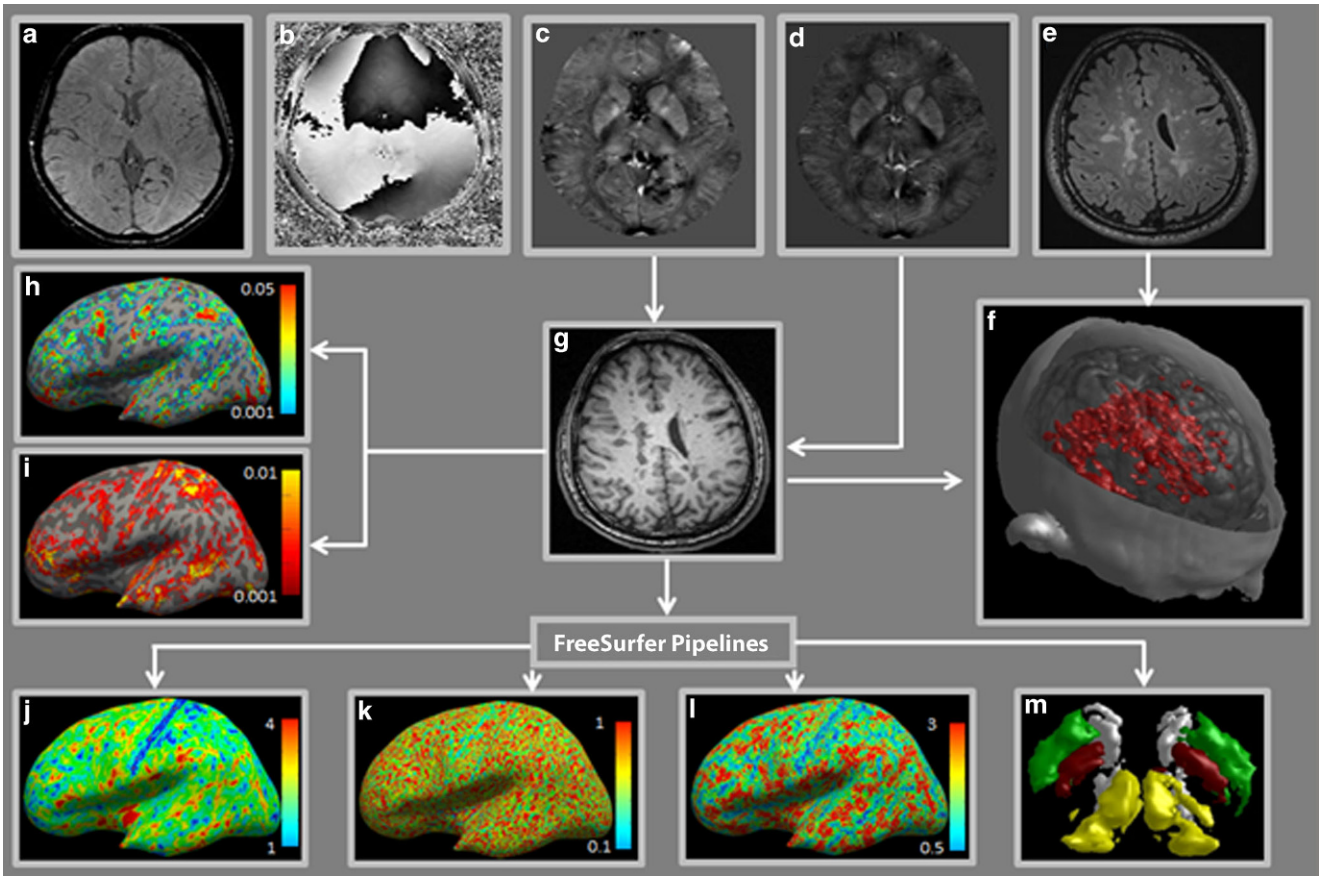

Fig. 1 Processing stream for structural MRI data: **a** magnitude data, **b** phase data, **c** unwrapped filtered phase image, **d** magnetic susceptibility map, **e** T2-FLAIR image, **f** 3D rendering of segmented T2-lesions, **g** high-resolution T1-weighted image, **h** cortical magnetic susceptibility mapping, **i** cortical iron mapping, **j** cortical thickness mapping, **k** cortical surface area mapping, **l** cortical volume mapping and **m** 3D rendering of segmented deep grey matter structures

as the sum of all segmented lesion volumes from all slices. The extracted MS lesions were converted into a mask and used to extract the magnetic susceptibility and phase values of these MS lesions from the magnetic susceptibility and the filtered phase maps, respectively. The lesion phase values relative to those of CSF were used to estimate the MS lesion iron concentration [32]. At a later stage, the white matter lesion masks were used in FSL (www.fmrib.ox.ac.uk/fsl/) to fill their corresponding white lesions holes using the intensity of neighboring normal-appearing WM before feeding the images into the FreeSurfer in order to avoid bias in tissue automatic segmentation [33].

Cortical Reconstruction and Volumetric Segmentation in FreeSurfer

Cortical reconstruction and volumetric segmentation were performed with the FreeSurfer image analysis suite (http://surfer.nmr.mgh.harvard.edu/). The technical details of these procedures are described elsewhere [34–36] and involve segmenting volumetric MRI images into grey, white, and cerebrospinal fluid. The deep grey matter in each hemisphere is segmented into seven subcortical structures, i.e. caudate nucleus (CN), putamen (PT), globus pallidus (GP), thalamus (TH), hippocampus, amygdala, and nucleus accumbens, followed by the calculation of their volumes. Thereafter, the cortical grey/white boundary is estimated by classifying all white matter voxels in an MRI volume and the surface of the connected white matter voxels is refined to obtain sub-voxel accuracy of the grey/white boundary. Furthermore, the pial surface is constructed by outwardly deforming the white/grey boundary. The FreeSurfer calculates the cortical thickness as the perpendicular distance between these two surfaces at each spatial cortical location and subsequently outputs the areas of each of these surfaces in mm^2. Finally, the cortical surface is parcellated into discrete units based on gyral and sulcal anatomy. All processed brains images were visually inspected for any topological defects, geometric inaccuracy due to brain lesions and any other visible defects. Manual editing for these deficits was done and the segmentation process was re-started.

Table 2 Morphometric measurements, magnetic susceptibility, and iron concentration of cortical and subcortical grey matter structures

	RRMS	Controls	
	Mean ± SD	Mean ± SD	*p*-value
Grey matter morphometric measures			
Cortical thickness (mm)	2.277 ± 0.077	2.346 ± 0.105	<0.01
Cortical area (mm^2)	0.162 ± 0.019	0.143 ± 0.025	<0.01
Normalized cortical volume	0.366 ± 0.045	0.420 ± 0.062	<0.01
Normalized CN volume	0.006 ± 0.001	0.008 ± 0.001	<0.01
Normalized PT volume	0.008 ± 0.001	0.011 ± 0.002	<0.01
Normalized GP volume	0.002 ± 0.0005	0.003 ± 0.0006	<0.01
Normalized TH volume	0.011 ± 0.002	0.015 ± 0.002	<0.01
Mean magnetic susceptibility ± SD (ppm)			
Cortex	0.0044 ± 0.003	0.0043 ± 0.004	–
CN	0.0338 ± 0.013	0.0286 ± 0.008	<0.05
PT	0.0199 ± 0.014	0.0183 ± 0.010	–
GP	0.110 ± 0.024	0.1026 ± 0.028	<0.05
TH	0.0086 ± 0.008	0.0089 ± 0.006	–
Mean iron concentration ± SD (μg)			
Cortex	1030.91 ± 496.21	729.86 ± 280.00	<0.01
CN	36.11 ± 10.86	34.03 ± 18.45	–
PT	75.97 ± 20.75	58.30 ± 19.15	<0.01
GP	23.41 ± 11.22	18.02 ± 7.26	<0.05
TH	69.31 ± 23.77	82.23 ± 26.94	<0.05

RRMS relapsing-remitting multiple sclerosis, *SD* standard deviation, *CN* caudate nucleus, *PT* putamen, *GP* globus pallidus, *TH* thalamus, *ppm* parts per million

Table 3 Pearson's correlation of the EDSS, time since diagnosis with some cortical and subcortical grey and white matter measurements in MS patients

	EDSS		Time since diagnosis (months)	
	r	*p*-value	r	*p*-value
Cortical thickness (mm)	–0.466	<0.01	–0.290	–
Cortical area (mm^2)	–0.126	<0.05	–0.085	–
Normalized cortical volume	–0.252	<0.05	–0.173	–
Normalized CN volume	–0.148	–	–0.002	–
Normalized PT volume	–0.267	–	–0.184	–
Normalized GP volume	–0.134	–	–0.170	–
Normalized TH volume	–0.290	–	–0.270	–
Magnetic susceptibility of the cortical ribbon (ppm)	0.436	<0.01	–0.133	–
Magnetic susceptibility of the CN (ppm)	0.213	–	0.014	–
Magnetic susceptibility of the PT (ppm)	0.331	<0.05	0.242	–
Magnetic susceptibility of the GP (ppm)	0.129	–	0.323	<0.05
Magnetic susceptibility of the TH (ppm)	0.045	–	0.223	–
Iron concentration of the cortical ribbon (ppm)	0.343	<0.05	–0.140	–
Iron concentration of the CN (μg)	0.442	<0.01	0.452	<0.01
Iron concentration of the PT (μg)	0.029	–	0.078	–
Iron concentration of the GP (μg)	0.006	–	–0.019	–
Iron concentration of the TH (μg)	0.183	–	–0.027	–
T2 lesion load (mm^3)	0.363	<0.05	0.192	–
Magnetic susceptibility of T2 lesions (ppm)	0.009	–	0.292	–
Iron concentration of T2 lesions (μg)	0.427	<0.05	0.295	–

EDSS expanded disability status scale, *DD* disease duration, *CN* caudate nucleus, *PT* putamen, *GP* globus pallidus, *TH* thalamus, *ppm* parts per million

To extract the cortical grey matter, subcortical white matter, and deep grey matter structures from other quantitative maps (magnetic susceptibility, filtered phase, and iron maps), the FreeSurfer-segmented left and right cortices (ribbons), and deep grey matter structures were mapped (converted) from the conformed FreeSurfer space to the native anatomical space "rawavg" space. Furthermore, each of these segmented structures was thresholded (using the structure's label value provided in the FreeSurfer's Look-Up-Table, LUT) and binarized to extract the corresponding anatomy from the magnetic susceptibility, filtered phase, and iron maps.

Statistical Analyses

All statistical analyses were performed in SPSS 22 (SPSS, Chicago, IL). Differences between patients and controls were assessed using independent samples t-test. Correlation coefficients were calculated using Pearson's correlation. For the surface-based analyses, a general linear model was fitted at each vertex, using cortical thickness, surface area and volume as dependent variables. Cortical maps were smoothed using a 10 mm full width at half maximum (FWHM) Gaussian kernel. The general linear model was computed vertex by vertex for each hemisphere. The differences between patients and controls were investigated using gender and age as covariates. Corresponding surface analyses were done for each hemisphere for the associations between each cortical measure (thickness, surface area, and volume) and the EDSS, T2 lesion load, cortical magnetic susceptibility, and cortical iron concentration using a general linear model. Results were corrected for multiple comparisons using Z Monte Carlo simulation, with a threshold of $p < 0.05$ and 10,000 iterations, to provide cluster-wise correction for multiple comparisons across the surface.

Results

Table 2 shows that there were statistically significant ($p < 0.01$) differences between RRMS patients and healthy controls when they were compared for the mean cortical thickness, cortical surface area, iron concentration in the cortex and putamen, normalized cortical and subcortical grey matter (CN, PT, GP, and TH) volumes. Furthermore, the mean magnetic susceptibility in the CN and GP, as well as the iron concentration in the GP and TH were significantly different at $p < 0.05$ (Fig. 2). The statistically significant ($p < 0.05$) regional differences between RRMS patients and healthy controls for the cortical thickness, surface area and volume is demonstrated in Fig. 3. Regional differences in cortical thickness were found in the superior-parietal, superior-temporal, supra-marginal, middle-temporal regions of the left hemisphere. No significant regional differences were observed in cortical thickness between RRMS patients and healthy controls in any region of the right hemisphere. For the cortical surface area, the postcentral, inferior-parietal, rostral-middle-frontal, lateral-occipital regions of the left hemisphere were identified to show a statistically significant difference between RRMS patients and healthy controls with the patients having a smaller cortical surface area in these regions; however, only the superior-parietal region of the right hemisphere of the RRMS patients showed a statistically significant reduction in cortical surface area compared to those of healthy controls. Furthermore, different cortical regions in the left hemisphere showed a statistically significant reduction in the cortical volume of the RRMS patients when compared to those of the healthy controls. These include the postcentral, rostral-middle-frontal, lateral-occipital, inferior-parietal regions of the left hemisphere. Similar to the cortical area, only the superior-parietal region of the right hemisphere of the RRMS patients showed a statistically significant reduction in the cortical volume compared to healthy controls.

Findings illustrated in Table 3 revealed that EDSS had significant weak to moderate positive correlation with the mean magnetic susceptibility in the cortex ($r = 0.436$, $p < 0.01$) and putamen ($r = 0.331$, $p < 0.05$), and with mean iron concentration in the cortex ($r = 0.343$, $p < 0.05$), caudate nucleus ($r = 0.442$, $p < 0.01$), and T2 lesions ($r = 0.427$, $p < 0.05$). In addition, the EDSS scores showed a significant weak to moderate positive correlation with the white matter T2 lesion load ($r = 0.363$, $p < 0.05$). In contrast, EDSS scores had a significant weak to moderate negative correlation with the mean cortical thickness ($r = –0.466$, $p < 0.01$), cortical surface area ($r = –0.126$, $p < 0.05$), and cortical volume ($r = –0.252$, $p < 0.05$). Fig. 4 shows different cortical regions where the EDSS scores were significantly associated with reduced cortical thickness, cortical surface area, and cortical volume. Time since diagnosis showed a statistically significant weak to moderate positive correlation with the mean magnetic susceptibility in the globus pallidus ($r = 0.323$, $p < 0.05$), and iron concentration in the cortex ($r = 0.452$, $p < 0.01$).

Results in Table 4 revealed that all deep grey matter (CN, PT, GP, and TH) normalized volumes showed statistically significant ($p < 0.01$) strong positive correlation with the cortical surface area and volume in RRMS patients and healthy controls. Furthermore, cortical surface area of the RRMS patients had a significant negative correlation with the lesion load ($r = –0.208$, $p < 0.05$) and mean magnetic susceptibility of the cortex ($r = –0.408$, $p < 0.05$), while that of the healthy controls showed a significant negative correlation with the mean magnetic susceptibility of the cortex ($r = –0.362$, $p < 0.05$), thalamus ($r = –0.452$, $p < 0.05$), and the iron concentration in the GP ($r = –0.476$, $p < 0.01$).

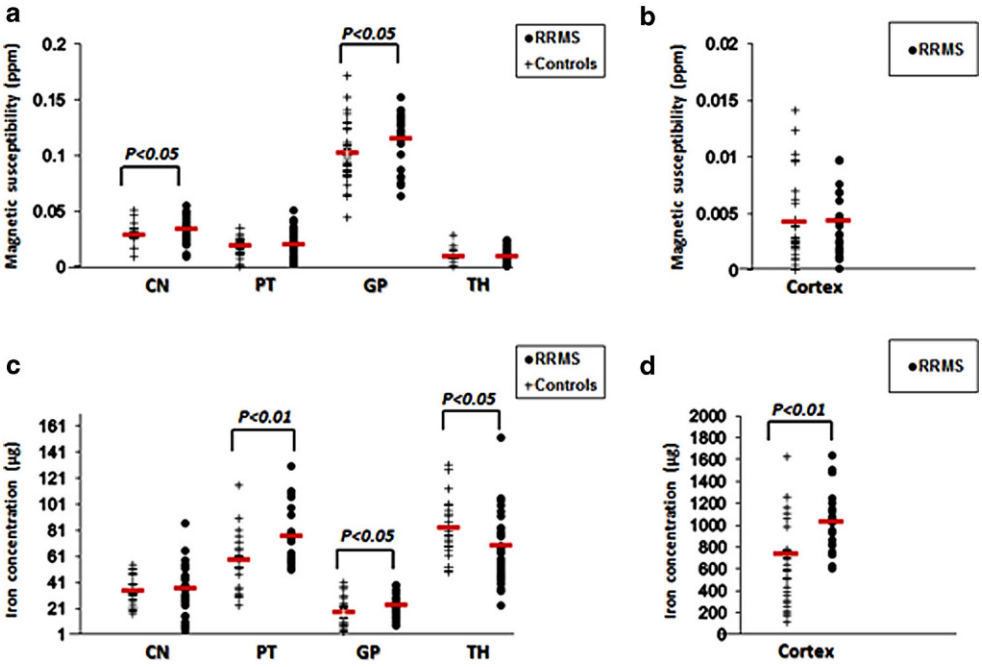

Fig. 2 Differences in the magnetic susceptibility (**a, b**) and iron concentration (**c, d**) of subcortical and cortical grey matter relative to the CSF, for all subjects in both study groups

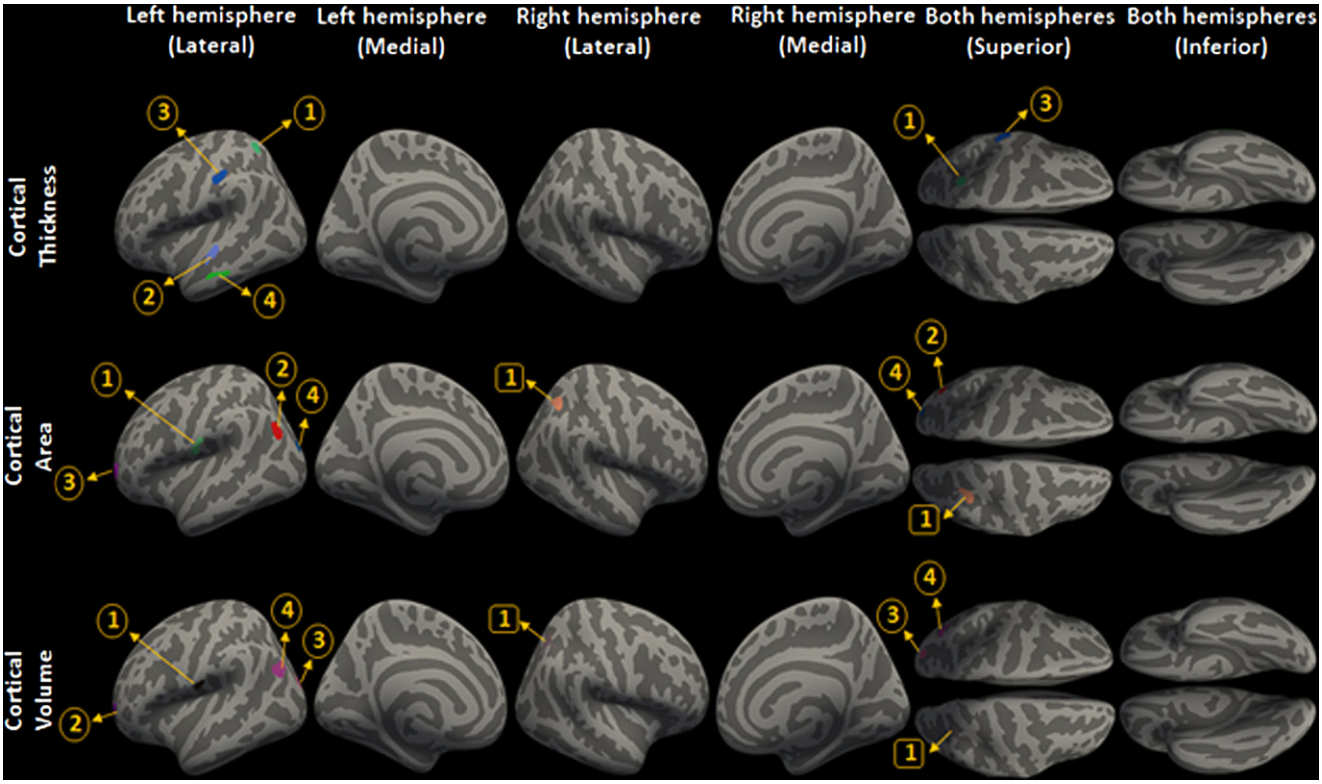

Fig. 3 Between-group surface-based differences in cortical thickness (*first row*), surface area (*second row*), and volume (*third row*). *Highlighted colors* represent regions (clusters of voxels) with statistically significant reduction in cortical thickness, area or volume in MS patients compared to healthy controls. The *highlighted regions* in the *first row* (cortical thickness) are: *1* superior-parietal, *2* superior-temporal, *3* supra-marginal, *4* middle temporal of the left hemisphere. The *highlighted regions* in the *second row* (cortical area) are: *1* post-central, *2* inferior-parietal, *3* rostral middle frontal, *4* lateral-occipital of the left hemisphere, and only one highlighted region (*1* superior-parietal) of the right hemisphere. The *highlighted regions* in the *third row* (cortical volume) are: *1* post-central, *2* rostral middle frontal, *3* lateral-occipital, *4* inferior-parietal of the left hemisphere, and only one *highlighted region* (*1* superior-parietal) of the right hemisphere. Results were obtained using Monte Carlo simulation, with a threshold of $p < 0.05$, to provide cluster-wise correction for multiple comparisons

Table 4 Pearson's correlations of the cortical thickness, surface area, and volume with different measures in MS patients and healthy controls

	RRMS						Controls					
	Cortical thickness (mm)		Cortical area (mm^2)		Normalized cortical volume		Cortical thickness (mm)		Cortical area (mm^2)		Normalized cortical volume	
	r	*p*	r	*p*	r	*p*	r	*p*	r	*p*	r	*p*
Age (years)	–0.75	<0.01	–0.149	–	–0.331	–	–0.240	–	–0.165	–	–0.257	–
EDSS	–0.466	<0.01	–0.126	<0.05	–0.252	<0.05	–	–	–	–	–	–
Time since diagnosis (months)	–0.290	–	–0.085	–	–0.173	–	–	–	–	–	–	–
Cortical susceptibility (ppm)	–0.113	<0.05	–0.408	<0.05	–0.410	<0.05	–0.297	–	–0.362	<0.05	–0.312	–
CN susceptibility (ppm)	–0.055	–	–0.08	–	–0.044	–	–0.07	–	–0.164	–	–0.208	–
PT susceptibility (ppm)	–0.411	<0.05	–0.139	–	–0.287	–	–0.341	–	–0.104	–	–0.019	–
GP Susceptibility (ppm)	–0.160	–	–0.065	–	–0.051	–	–0.206	–	–0.164	–	–0.251	–
TH susceptibility (ppm)	–0.116	–	–0.125	–	–0.190	–	–0.290	–	–0.452	<0.05	–0.395	<0.05
Cortical iron (μg)	–0.430	<0.05	–0.328	–	–0.304	–	–0.034	–	–0.002	–	–0.012	–
CN iron (μg)	–0.282	–	–0.298	–	–0.386	<0.05	–0.171	–	–0.052	–	–0.009	–
PT iron (μg)	–0.038	–	–0.095	–	–0.068	–	–0.245	–	–0.093	–	–0.03	–
GP iron (μg)	–0.191	–	–0.060	–	–0.01	–	–0.007	–	–0.476	<0.01	–0.531	<0.01
TH iron (μg)	–0.213	–	–0.229	–	–0.3	–	–0.243	–	–0.146	–	–0.117	–
Normalized CN volume	0.034	–	0.782	<0.01	0.824	<0.01	0.206	–	0.787	<0.01	0.780	<0.01
Normalized PT volume	0.074	–	0.84	<0.01	0.873	<0.01	0.350	–	0.848	<0.01	0.816	<0.01
Normalized GP volume	0.019	–	0.878	<0.01	0.893	<0.01	0.138	–	0.828	<0.01	0.863	<0.01
Normalized TH volume	0.097	–	0.903	<0.01	0.938	<0.01	0.269	–	0.923	<0.01	0.902	<0.01
T2 lesion Load (mm^3)	–0.294	<0.05	–0.208	<0.05	–0.245	<0.05	–	–	–	–	–	–
T2 lesion magnetic susceptibility (ppm)	–0.255	–	–0.162	–	–0.069	–	–	–	–	–	–	–
T2 lesion iron (μg)	–0.342	–	–0.24	–	–0.303	–	–	–	–	–	–	–

CN caudate nucleus, *PT* putamen, *GP* globus pallidus, *TH* thalamus

On the other hand, cortical volume of the RRMS patients had a significant negative correlation with the lesion load (r = –0.245, $p < 0.05$), mean magnetic susceptibility of the cortex (r = –0.410, $p < 0.05$), and iron concentration in the caudate nucleus (r = –0.386, $p < 0.05$), while it revealed a significant negative correlation with the mean magnetic susceptibility of the thalamus (r = –0.395, $p < 0.05$), and iron concentration in the globus pallidus (r = –0.531, $p < 0.01$) in healthy controls. For the cortical thickness, it had significant negative correlations with the age (r = –0.75, $p < 0.01$), lesion T2 load (r = –0.294, $p < 0.05$), mean magnetic susceptibility of the cortex (r = –0.113, $p < 0.05$), putamen (r = –0.411, $p < 0.05$) and iron concentration in the cortex (r = –0.430, $p < 0.05$) in RRMS patients only. Different cortical regions showed a significant association between the magnetic susceptibility and the reduced cortical thickness, cortical surface area, and cortical volume as shown in Fig. S1 (Online Resource 1). Furthermore, only the reduced cortical thickness was found to associate with the cortical iron concentration as shown in Fig. S2 (Online Resource 1).

Table 5 revealed that white matter T2 lesion load had a significant ($p < 0.05$) weak to moderate negative correlation with the normalized cortical (r = –0.245), putamen (r = –0.408), globus pallidus (r = –0.410) and thalamus (r =

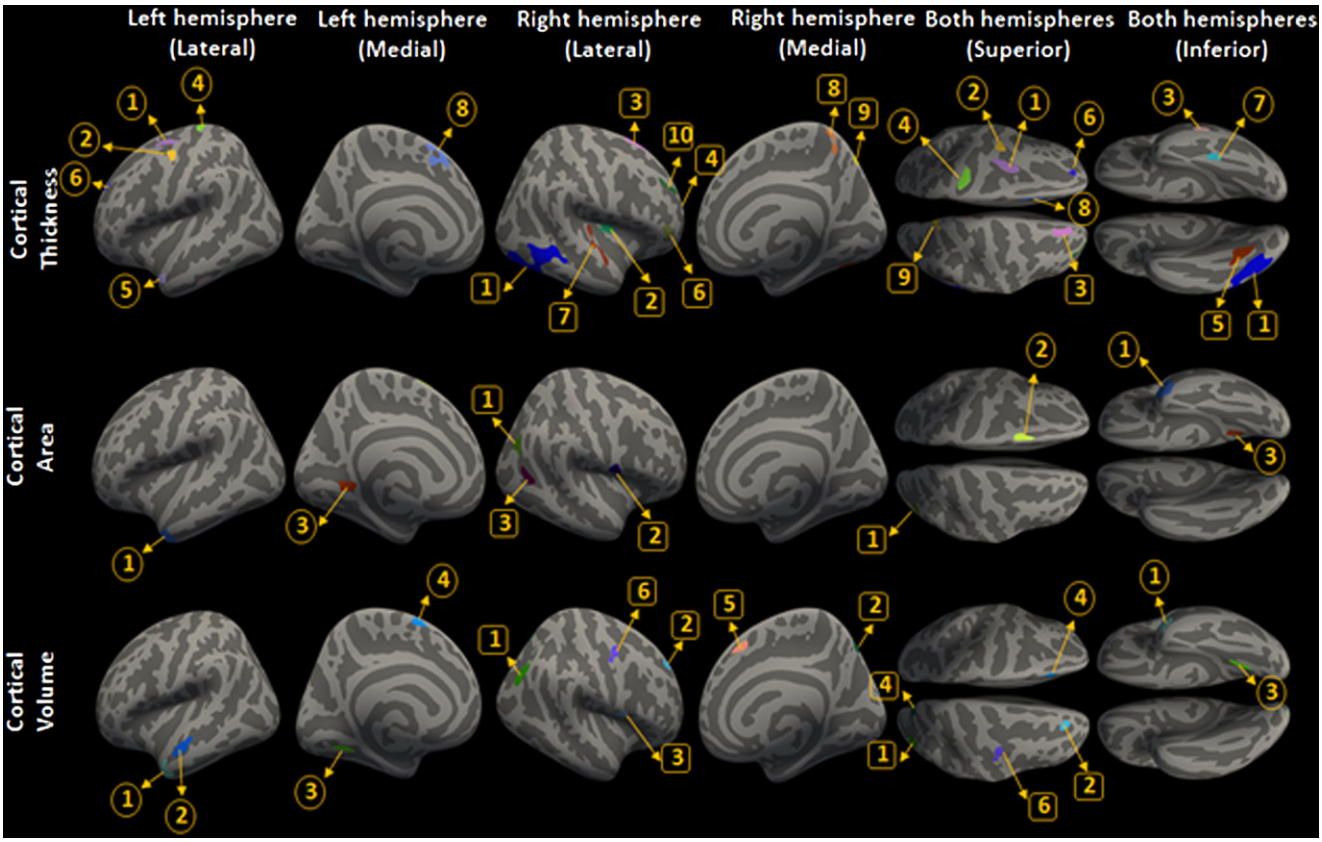

Fig. 4 Regions of statistically significant correlations of EDSS with cortical thickness (*first row*), surface area (*second row*), and volume (*third row*). The *highlighted regions* in the *first row* (cortical thickness) are: *1* caudal-middle-frontal, *2* pre-central, *3* inferior-temporal, *4* pre-central, *5* superior-temporal, *6* rostral-middle-frontal, *7* fusiform, *8* superior-frontal of the left hemisphere, and *1* middle temporal, *2* insula, *3* superior-frontal, *4* rostral middle frontal, *5* fusiform, *6* pars triangularis, *7* superior-temporal, *8* precuneus, *9* superior-parietal, *10* rostral middle frontal of the right hemisphere. The *highlighted regions* in the *second row* (cortical area) are: *1* temporal pole, *2* superior-frontal, *3* lingual of the left hemisphere, and *1* inferior-parietal, *2* precentral, *3* inferior-parietal of the right hemisphere. The *highlighted regions* in the *third row* (cortical volume) are: *1* middle temporal, *2* superior-temporal, *3* lingual, *4* superior-frontal, and *1* inferior-parietal, *2* superior-frontal, *3* precentral, *4* superior-parietal, *5* superior-frontal, *6* precentral of the right hemisphere. Results were obtained using Monte Carlo simulation, with a threshold of $p < 0.05$, to provide cluster-wise correction for multiple comparisons

–0.407) volumes. Fig. 5 shows that the reduced cortical thickness, cortical surface area and volume were associated with the lesion load in different cortical areas. Furthermore, white matter T2 lesion load showed a significant weak to moderate positive correlation with the mean magnetic susceptibility in the cortex ($r = 0.648$, $p < 0.01$) globus pallidus ($r = 0.318$, $p < 0.05$) and iron concentration in the cortex ($r = 0.488$, $p < 0.01$).

Discussion

In the present study, global and regional morphometric (thickness, surface area, and volume) changes and iron accumulation in the cortical and subcortical grey matter structures were investigated and compared between a group of RRMS patients and age-matched healthy controls and tested for any possible associations within each group of subjects. In RRMS patients, white matter T2 lesion load, EDSS, and time since diagnosis were also tested for any possible association with all morphometric, iron and magnetic susceptibility values measured in the cortex, deep grey matter structures and white matter T2 lesions. In addition, surface-based analyses were performed in FreeSurfer for each hemisphere in both groups of subjects to look at the spatial distribution of cortical morphometric, magnetic susceptibility and iron changes. Findings from the present study showed that there were statistically significant differences between the RRMS patients and age-matched healthy controls for cortical thickness, surface area and volume. It was obvious that cortical thicknesses of the parietal (superior-parietal and supramarginal gyri) and temporal (superior-temporal and middle-temporal gyri) lobes of the left hemisphere were significantly thinner in RRMS as compared to healthy controls. These findings are partly similar to those reported in other studies [37–40] in which thickness dif-

Table 5 Pearson's correlations of the T2 lesions load with the morphometric measurements of the cortical and subcortical grey matter, magnetic susceptibility and iron concentration in RRMS patients

	r	*p*-value
Cortical thickness (mm)	–0.294	<0.05
Cortical area (mm^2)	–0.208	<0.05
Normalized cortical volume	–0.245	<0.05
Normalized CN volume	–0.194	–
Normalized PT volume	–0.408	<0.05
Normalized GP volume	–0.410	<0.05
Normalized TH volume	–0.407	<0.05
Magnetic susceptibility of the cortical ribbon (ppm)	0.648	<0.01
Magnetic susceptibility of the CN (ppm)	0.084	–
Magnetic susceptibility of the PT (ppm)	0.110	–
Magnetic susceptibility of the GP (ppm)	0.318	<0.05
Magnetic susceptibility of the TH (ppm)	0.032	–
Iron concentration of the cortical ribbon (μg)	0.488	<0.01
Iron concentration of the CN (μg)	0.262	–
Iron concentration of the PT (μg)	0.200	–
Iron concentration of the GP (μg)	0.007	–
Iron concentration of the TH (μg)	0.258	–

RRMS relapsing-remitting multiple sclerosis, *CN* caudate nucleus, *PT* putamen, *GP* globus pallidus, *TH* thalamus, *ppm* parts per million

ferences were larger and more widespread to include the occipital and frontal lobes as well [37–40]. Interestingly, cortical surface areas of the parietal (postcentral and inferior-parietal gyri), frontal (rostral-middle-frontal gyrus) and occipital (lateral-occipital gyrus) lobes of the left hemisphere, as well as the parietal (superior-parietal gyrus) lobe of the right hemisphere of the RRMS patients were found to be reduced when compared to those in healthy controls. To our knowledge, only two studies have previously evaluated the cortical surface area in MS [40, 41] and only one found significant differences in single hemisphere surface area between MS patients and healthy controls [41]. Results from the current study also showed a significant decrease in cortical volume in the parietal (postcentral and inferior-parietal gyri), frontal (rostral-middle-frontal), and occipital (lateral-occipital) lobes of the left hemisphere, as well as the parietal (superior-parietal) lobe of the right hemisphere of the RRMS patients as compared to healthy controls. These regions were different from those found by Nygaard et al. [40], as they found volume differences in the pre-central, post-central, in the superior parietal regions bilaterally, and in the superior and orbital frontal regions of the left hemisphere. In a study by Charil et al. [42], it was found that loss of cortical volume in MS does not occur in a uniform pattern, and it is seen more often in specific regions such as the cingulate gyrus and insular regions.

In this study, volumetric measurements of the deep grey matter structures (caudate nucleus, putamen, globus pallidus, and thalamus) of the RRMS revealed a significant atrophy when compared to those of the age-matched healthy controls. These findings are in agreement with those reported in a recent study by Datta et al. [43]. Furthermore, volumetric measurements in the present study showed that deep grey matter volumes were significantly associated with morphometric changes in the cortical thickness, surface area and volume, revealing a strong connection between the cortical and subcortical grey matter atrophy. The cortical and subcortical morphometric changes reported in this study show that the grey matter is very much involved in the MS disease process and substantial neurodegeneration is undergone during the relapsing-remitting phase of the disease. Our findings showed a significant weak to moderate correlation between the cerebral cortex atrophy and the EDSS, a method of quantifying disability in MS. No association was detected between any of the volumetric changes in the deep grey matter and the EDSS. Filippi et al. found that clinical disability is associated more with cortical pathology than with T2-lesions or normal appearing white matter [44]. Furthermore, it was also reported that MS progression was associated with cortical atrophy and subcortical grey matter changes [45, 46].

In RRMS patients, the caudate nucleus and globus pallidus were the only two deep grey matter structures studied that had significantly increased magnetic susceptibility, as assessed by MR susceptibility mapping, as compared to the healthy control subjects. No significant increase in the magnetic susceptibility in the cortex of the RRMS patients was observed. Iron concentration, on the other hand, was derived from the phase shift in each of these grey matter regions (cortical and subcortical) relative to the mean phase value of the CSF according to the equation proposed by Haacke et al. [30]. With the exception of the caudate nucleus, a sig-

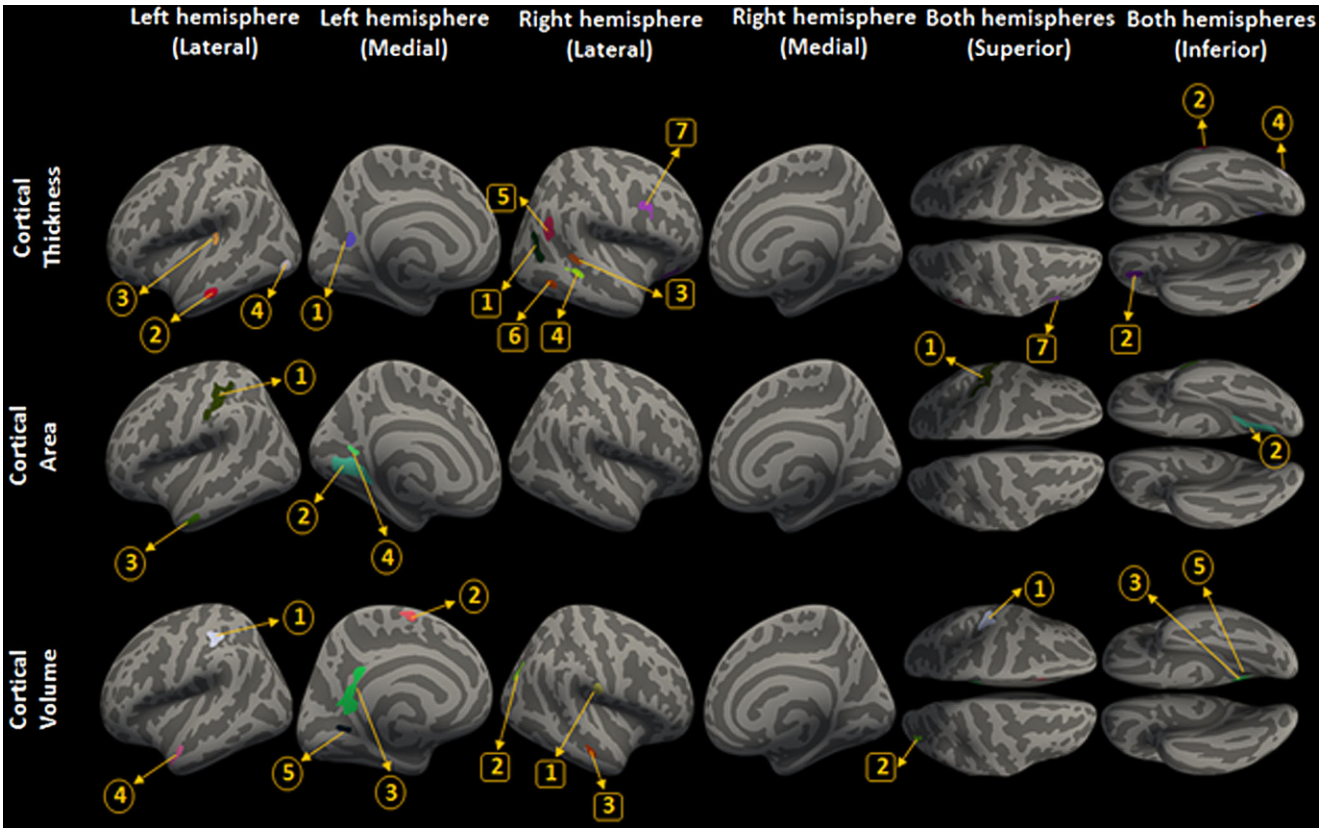

Fig. 5 Regions of statistically significant correlations of Lesion Load with cortical thickness (*first row*), area (*second row*), and volume (*third row*). The *highlighted regions* in the *first row* (cortical thickness) are: *1* precuneus, *2* middle-temporal, *3* superior-temporal, *4* lateral-occipital of the left hemisphere, and *1* inferior-parietal, *2* lateral-orbitofrontal, *3* bankssts (banks of the superior temporal sulcus), *4* bankssts, *5* inferior-parietal, *6* inferior-temporal, *7* caudal middle frontal of the right hemisphere. The *highlighted regions* in the *second row* (cortical area) are: *1* supra-marginal, *2* lingual, *3* middle temporal, *4* precuneus of left hemisphere, and only one highlighted region (1 middle temporal) of the right hemisphere. The *highlighted regions* in the *third row* (cortical volume) are: *1* supra-marginal, *2* superior-frontal, *3* isthmus of cingulate, *4* superior-temporal, *5* lingual of the left hemisphere, and *1* post-central, *2* inferior-parietal, *3* middle temporal of the right hemisphere. Results were obtained using Monte Carlo simulation, with a threshold of $p < 0.05$, to provide cluster-wise correction for multiple comparisons

nificant increase was observed in the cerebral cortex and all other deep grey matter regions studied. This suggested that iron accumulation occurred in the cerebral cortex and most dGM regions in the relapsing-remitting phase of demyelinating disease or even earlier as reported previously [20]. These findings are in agreement with those reported in some previous studies [47–49]; however, it is known that phase images are distorted by a non-local relationship between the underlying susceptibility distribution and the resulting field perturbation, which gives rise to the phase shifts [28] and this non-local relationship can be corrected by using quantitative susceptibility mapping (QSM) techniques. In addition, the phase is known to be very sensitive to subtle changes in the magnetic or frequency shift and thus very sensitive to very low concentrations of iron content, but it underestimates iron content due to the phase aliasing, that occurs when iron concentration is too high [32]. It should also be noted that although tissue susceptibility and phase shift are likely to be dominated by iron in these structures, the susceptibility of tissue depends on more than just the iron content. It has been shown that susceptibility offset is highly dependent on the underlying orientation of nerve fibers relative to the main magnetic field (B_0) [50]. In addition, findings in this study showed a significant inverse weak to moderate association between the cortical morphometric changes and the cortical magnetic susceptibility. The surface-based analysis showed that the reduction in cortical thickness in some cortical regions in the left hemisphere (insula, isthmus cingulate, middle-temporal, postcentral, temporal pole) and the right hemisphere (superior-parietal, and lateral-orbitofrontal) were significantly associated with the increased magnetic susceptibility in these regions; however, the reduction of both cortical surface area and volume of the precuneus and inferior-parietal cortical regions of the left hemisphere was negatively associated with the increased magnetic susceptibility. On the other hand, only the cortical thickness showed a significant inverse moderate correlation with the iron concentration in the cerebral cortex and such

association was localized to the superior-frontal gyrus of the left hemisphere, and the rostral-anterior-cingulate, rostral-middle-frontal, and rostral-middle-frontal of the right hemisphere. No significant correlation was found between any of the cortical morphometric measures and the magnetic susceptibility or iron concentration in the T2 lesions suggesting either different pathological processes that lead to iron deposition in these lesions or a different rate of iron deposition from that in the cortical grey matter. Iron concentration measured in the cerebral cortex, caudate nucleus and white matter lesions, as well as the magnetic susceptibility measured in the cerebral cortex and the putamen, showed moderate positive correlation with the EDSS.

It was obvious that white matter T2 lesion load showed significant weak to moderate negative association with the morphometric measurements used in this study in all cortical and subcortical grey matter regions except for the caudate nucleus. The negative association between the T2 lesion load and cortical thickness was localized to the parietal (precuneus), temporal (middle-temporal, superior-temporal, and cortical areas around superior temporal sulcus), and occipital (lateral-occipital) lobes of the left hemisphere, and the frontal (lateral-orbitofrontal and caudal-middle-frontal), parietal (inferior-parietal and inferior-parietal), and temporal (inferior-temporal) lobes of the right hemisphere. Similarly, the parietal (precuneus, supramarginal), temporal (middle-temporal), and occipital (lingual) lobes of the left hemisphere, and the temporal (middle-temporal) lobe of the right hemisphere showed a negative association with the T2 lesion load.; however, the association between the lesion load and cortical volume was restricted to some regions within the left hemisphere (superior-frontal, supramarginal, superior-temporal, lingual, and isthmus cingulate) and the right hemisphere (postcentral, inferior-parietal, middle-temporal) of the RRMS patients. Furthermore, a positive correlation between the white matter T2 lesion load and iron concentration in the cerebral cortex is another important finding in this study. Except for the globus pallidus, no significant association was found between either the magnetic susceptibility or the iron deposition in the dGM structures and the T2 lesion load. These results do not agree with previous findings by Raz et al. [27]. Our findings also showed a significant moderate association between the lesion load and the EDSS. These findings together reveal that white matter T2 lesion load is associated with the grey matter atrophy, disability, and cortical iron, and they are in agreement with previously reported results by Charil et al. as they found a significant association between the mean cortical thickness, lesion load and the EDSS [42].

To our knowledge, this is the first study to assess the iron deposition in the cerebral cortex in RRMS patients in vivo. The increased cortical iron deposition has only been seen in postmortem studies of neurodegenerative diseases and healthy aging [21–24], and only one in vivo study of cerebral iron deposition was performed in a group of healthy aging volunteers [25]. This was attributed to the complexity of cortical ribbon and its relatively low iron content.

The results of the present work showed that cortical grey matter changes tend to occur preferentially in the left hemisphere of the MS brains of the present study. Although the majority of studies did not directly evaluate the presence of asymmetry in hemispheric involvement in the MS disease, some studies showed a preferential cortical left-sided GM loss in RRMS patients [51, 52], and this finding was confirmed by the lateralization index (LI), a quantification measure of the hemisphere asymmetry [53]. These studies suggest that the left hemisphere might be more susceptible to the accumulation of damage. The left hemisphere is dominant for both the language and handedness in the majority of right-handed subjects, and this may partially explain the preferential cortical left-sided GM changes in the present study, as the majority of our patients (26/30) were right-handed. One possible explanation for the asymmetric involvement of left hemisphere in cortical grey matter changes is the high susceptibility of the left hemisphere to neural and metabolic dysfunction, which might be attributed to its overuse in the right-handed subjects.

To the best of our knowledge, this is the first study to investigate the cortical and subcortical grey matter in a multiparametric approach using a composite from a combination of MRI measures (cortical and subcortical morphometric measurements, iron deposition and magnetic susceptibility), and to link these grey matter measures to the white matter T2 lesion load to capture different aspects of the MS disease during the relapsing-remitting phase. Furthermore, it is the first study to assess the cortical iron in RRMS patients, as the increased cortical iron deposition has only been seen in postmortem studies of neurodegenerative diseases and healthy aging [21–24], and in vivo in a group of healthy aging subjects using the phase images of T2*-weighted images at ultra-high field MRI (7 T; [25]). This was attributed to the complexity of cortical ribbon and its relatively low iron content; however, the main limitation of the current study was the relatively small sample size. So, additional studies with a larger number of RRMS patients and more MS phenotypes, such as primary and secondary progressive MS are required to validate these findings.

In conclusion, cortical and subcortical grey matter is very much involved in the MS disease process and quite substantial neurodegeneration is undergone during the relapsing-remitting phase of the disease. In addition, cortical morphometric changes occur in a non-uniform pattern and are very likely to be associated with cortical iron deposition and magnetic susceptibility, dGM atrophy, white matter T2 lesion load, and disability.

Acknowledgements We would like to thank the Royal Medical Services for their great help and support and for allowing us to use their 3T MRI to scan our patients and healthy controls.

Funding This research did not receive any specific grant from funding agencies in the public, commercial, or not-for-profit sectors.

Compliance with ethical guidelines

Conflict of interest A. Al-Radaideh, I. Athamneh, H. Alabadi and M. Hbahbih declare that they have no competing interests.

Ethical standards The present study was approved by the Royal Medical Service ethics committee and carried out in accordance with the code of ethics of the World Medical Association (Declaration of Helsinki). All participants were asked to sign a consent form and fill out the MRI safety questionnaire before participating in the study.

References

1. Compston A, Coles A. Multiple sclerosis. Lancet. 2008;372:1502–17.
2. Neema M, Stankiewicz J, Arora A, Dandamudi VS, Batt CE, Guss ZD, Al-Sabbagh A, Bakshi R. T1- and T2-based MRI measures of diffuse gray matter and white matter damage in patients with multiple sclerosis. J Neuroimaging. 2007;17:16S–21S.
3. Rovaris M, Rocca MA, Filippi M. Magnetic resonance-based techniques for the study and management of multiple sclerosis. Br Med Bull. 2003;65:133–44.
4. Bö L, Geurts JJ, van der Valk P, Polman C, Barkhof F. Lack of correlation between cortical demyelination and white matter pathologic changes in multiple sclerosis. Arch Neurol. 2007;64:76–80.
5. Klaver R, De Vries HE, Schenk GJ, Geurts JJ. Grey matter damage in multiple sclerosis. Prion. 2013;7:66–75.
6. Schutzer SE, Angel TE, Liu T, Schepmoes AA, Xie F, Bergquist J, Vécsei L, Zadori D, Camp DG 2nd, Holland BK, Smith RD, Coyle PK. Gray matter is targeted in first-attack multiple sclerosis. PLoS ONE. 2013;8:e66117.
7. Pirko I, Lucchinetti CF, Sriram S, Bakshi R. Gray matter involvement in multiple sclerosis. Neurology. 2007;68:634–42.
8. Dawson JW. The histology of multiple sclerosis. Philos Trans R Soc. 1916;50:517–740.
9. Kutzelnigg A1, Lucchinetti CF, Stadelmann C, Brück W, Rauschka H, Bergmann M, Schmidbauer M, Parisi JE, Lassmann H. Cortical demyelination and diffuse white matter injury in multiple sclerosis. Brain. 2005;128:2705–12.
10. Geurts JJ, Bö L, Pouwels PJ, Castelijns JA, Polman CH, Barkhof F. Cortical lesions in multiple sclerosis: combined postmortem MR imaging and histopathology. AJNR Am J Neuroradiol. 2005;26(3):572–7.
11. Kidd D, Barkhof F, McConnell R, Algra PR, Allen IV, Revesz T. Cortical lesions in multiple sclerosis. Brain. 1999;122:17–26.
12. Peterson JW, Bö L, Mörk S, Chang A, Trapp BD. Transected neurites, apoptotic neurons, and reduced inflammation in cortical multiple sclerosis lesions. Ann Neurol. 2001;50:389–400.
13. Wegner C, Esiri MM, Chance SA, Palace J, Matthews PM. Neocortical neuronal, synaptic, and glial loss in multiple sclerosis. Neurology. 2006;67:960–7.
14. Dutta R, Chang A, Doud MK, Kidd GJ, Ribaudo MV, Young EA, Fox RJ, Staugaitis SM, Trapp BD. Demyelination causes synaptic alterations in hippocampi from multiple sclerosis patients. Ann Neurol. 2011;69:445–54.
15. Bakshi R, Dandamudi VSR, Neema M, De C, Bermel RA. Measurement of brain and spinal cord atrophy by magnetic resonance imaging as a tool to monitor multiple sclerosis. J Neuroimaging. 2005;15(4 Suppl):30S-45S.
16. Fisher E, Lee JC, Nakamura K, Rudick RA. Gray matter atrophy in multiple sclerosis: a longitudinal study. Ann Neurol. 2008;64:255–65.
17. Zecca L, Youdim MB, Riederer P, Connor JR, Crichton RR. Iron, brain ageing and neurodegenerative disorders. Nat Rev Neurosci. 2004;5:863–73.
18. Sadrzadeh SM, Saffari Y. Iron and brain disorders. Am J Clin Pathol. 2004;121 Suppl:S64–70.
19. LeVine SM. Iron deposits in multiple sclerosis and Alzheimer's disease brains. Brain Res. 1997;760:298–303.
20. Al-Radaideh AM, Wharton SJ, Lim SY, Tench CR, Morgan PS, Bowtell RW, Constantinescu CS, Gowland PA. Increased iron accumulation occurs in the earliest stages of demyelinating disease: an ultra-high field susceptibility mapping study in Clinically Isolated Syndrome. Mult Scler. 2013;19:896–903.
21. Hallgren B, Sourander P. The effect of age on the non-haemin iron in the human brain. J Neurochem. 1958;3:41–51.
22. Hebbrecht G, Maenhaut W, De Reuck J. Brain trace elements and aging. Nucl Instrum Methods Phys Res B. 1999;150:208–13.
23. Ramos P, Santos A, Pinto NR, Mendes R, Magalhães T, Almeida A. Iron levels in the human brain: a post-mortem study of anatomical region differences and age-related changes. J Trace Elem Med Biol. 2014;28:13–7.
24. Yao B, Hametner S, van Gelderen P, Merkle H, Chen C, Lassmann H, Duyn JH, Bagnato F. 7 Tesla magnetic resonance imaging to detect cortical pathology in multiple sclerosis. PLoS ONE. 2014;9:e108863.
25. Buijs M, Doan NT, van Rooden S, Versluis MJ, van Lew B, Milles J, van der Grond J, van Buchem MA. In vivo assessment of iron content of the cerebral cortex in healthy aging using 7-Tesla T2*-weighted phase imaging. Neurobiol Aging. 2017;53:20–6.
26. Moodie J, Healy BC, Buckle GJ, Gauthier SA, Glanz BI, Arora A, Ceccarelli A, Tauhid S, Han XM, Venkataraman A, Chitnis T, Khoury SJ, Guttmann CR, Weiner HL, Neema M, Bakshi R. Magnetic resonance disease severity scale (MRDSS) for patients with multiple sclerosis: a longitudinal study. J Neurol Sci. 2012;315:49–54.
27. Raz E, Branson B, Jensen JH, Bester M, Babb JS, Herbert J, Grossman RI, Inglese M. Relationship between iron accumulation and white matter injury in multiple sclerosis: a case-control study. J Neurol. 2015;262:402–9.
28. Wharton S, Schäfer A, Bowtell R. Susceptibility mapping in the human brain using threshold-based k-space division. Magn Reson Med. 2010;63:1292–304.
29. Haacke EM, Ayaz M, Khan A, Manova ES, Krishnamurthy B, Gollapalli L, Ciulla C, Kim I, Petersen F, Kirsch W. Establishing a baseline phase behavior in magnetic resonance imaging to determine normal vs. abnormal iron content in the brain. J Magn Reson Imaging. 2007;26:256–64.
30. Susceptibility weighted imaging in MRI: basic concepts and clinical applications. Eds. EM Haacke, JR Reichenbach, John Wiley & Sons, 2014
31. Udupa JK, Samarasekera S. Fuzzy connectedness and object definition: theory, algorithms, and applications in image segmentation. Graph Models Image Process. 1996;58:246–61.
32. Liu M, Habib C, Miao Y, Haacke EM. Measuring iron content with phase. Susceptibility weighted imaging in MRI: basic concepts and clinical applications. Eds. EM Haacke, JR Reichenbach, pp. 369–401, John Wiley & Sons 2011.
33. Battaglini M, Jenkinson M, De Stefano N. Evaluating and reducing the impact of white matter lesions on brain volume measurements. Hum Brain Mapp. 2012;33:2062–71.
34. Fischl B, Salat DH, Busa E, Albert M, Dieterich M, Haselgrove C, van der Kouwe A, Killiany R, Kennedy D, Klaveness S, Montillo

A, Makris N, Rosen B, Dale AM. Whole brain segmentation: automated labeling of neuroanatomical structures in the human brain. Neuron. 2002;33:341–55.
35. Fischl B, Sereno MI, Dale AM. Cortical surface-based analysis. II: Inflation, flattening, and a surface-based coordinate system. Neuroimage. 1999;9:195–207.
36. Dale AM, Fischl B, Sereno MI. Cortical surface-based analysis. I. Segmentation and surface reconstruction. Neuroimage. 1999;9:179–94.
37. Sailer M, Fischl B, Salat D, Tempelmann C, Schönfeld MA, Busa E, Bodammer N, Heinze HJ, Dale A. Focal thinning of the cerebral cortex in multiple sclerosis. Brain. 2003;126:1734–44.
38. Narayana PA, Govindarajan KA, Goel P, Datta S, Lincoln JA, Cofield SS, Cutter GR, Lublin FD, Wolinsky JS; MRI Analysis Center at Houston; The CombiRx Investigators Group. Regional cortical thickness in relapsing remitting multiple sclerosis: a multicenter study. Neuroimage Clin. 2013;2:120–31.
39. Geisseler O, Pflugshaupt T, Bezzola L, Reuter K, Weller D, Schuknecht B, Brugger P, Linnebank M. Cortical thinning in the anterior cingulate cortex predicts multiple sclerosis patients' fluency performance in a lateralised manner. Neuroimage Clin. 2016;10:89–95.
40. Nygaard GO, Walhovd KB, Sowa P, Chepkoech JL, Bjørnerud A, Due-Tønnessen P, Landrø NI, Damangir S, Spulber G, Storsve AB, Beyer MK, Fjell AM, Celius EG, Harbo HF. Cortical thickness and surface area relate to specific symptoms in early relapsing-remitting multiple sclerosis. Mult Scler. 2015;21:402–14.
41. Hier DB, Wang J. Reduced cortical surface area in multiple sclerosis. Neurol Res. 2007;29:231–2.
42. Charil A, Dagher A, Lerch JP, Zijdenbos AP, Worsley KJ, Evans AC. Focal cortical atrophy in multiple sclerosis: relation to lesion load and disability. Neuroimage. 2007;34:509–17.
43. Datta S, Staewen TD, Cofield SS, Cutter GR, Lublin FD, Wolinsky JS, Narayana PA; MRI Analysis Center at Houston; CombiRx Investigators Group. Regional gray matter atrophy in relapsing remitting multiple sclerosis: baseline analysis of multi-center data. Mult Scler Relat Disord. 2015;4:124–36.
44. Filippi M, Rocca MA, Horsfield MA, Hametner S, Geurts JJ, Comi G, Lassmann H. Imaging cortical damage and dysfunction in multiple sclerosis. JAMA Neurol. 2013;70:556-64.
45. Filippi M, Preziosa P, Copetti M, Riccitelli G, Horsfield MA, Martinelli V, Comi G, Rocca MA. Gray matter damage predicts the accumulation of disability 13 years later in MS. Neurology. 2013;81:1759–67.
46. Jacobsen C, Hagemeier J, Myhr KM, Nyland H, Lode K, Bergsland N, Ramasamy DP, Dalaker TO, Larsen JP, Farbu E, Zivadinov R. Brain atrophy and disability progression in multiple sclerosis patients: a 10-year follow-up study. J Neurol Neurosurg Psychiatr. 2014;85:1109–15.
47. Hammond KE, Metcalf M, Carvajal L, Okuda DT, Srinivasan R, Vigneron D, Nelson SJ, Pelletier D. Quantitative in vivo magnetic resonance imaging of multiple sclerosis at 7 Tesla with sensitivity to iron. Ann Neurol. 2008;64:707–13.
48. Chen X, Zeng C, Luo T, Ouyang Y, Lv F, Rumzan R, Wang Z, Li Q, Wang J, Hou H, Huang F, Li Y. Iron deposition of the deep grey matter in patients with multiple sclerosis and neuromyelitis optica: a control quantitative study by 3D-enhanced susceptibility-weighted angiography (ESWAN). Eur J Radiol. 2012;81:e633–9.
49. Du S, Sah SK, Zeng C, Wang J, Liu Y, Xiong H, Li Y. Iron deposition in the gray matter in patients with relapse-remitting multiple sclerosis: a longitudinal study using three-dimensional (3D)-enhanced T2*-weighted angiography (ESWAN). Eur J Radiol. 2015;84:1325–32.
50. Lee J, Shmueli K, Fukunaga M, van Gelderen P, Merkle H, Silva AC, Duyn JH. Sensitivity of MRI resonance frequency to the orientation of brain tissue microstructure. Proc Natl Acad Sci U S A. 2010;107:5130-5.
51. Prinster A, Quarantelli M, Orefice G, Lanzillo R, Brunetti A, Mollica C, Salvatore E, Morra VB, Coppola G, Vacca G, Alfano B, Salvatore M. Grey matter loss in relapsing–remitting multiple sclerosis: a voxel-based morphometry study. Neuroimage. 2006;29:859–67.
52. Preziosa P, Pagani E, Mesaros S, Riccitelli GC, Dackovic J, Drulovic J, Filippi M, Rocca MA. Progression of regional atrophy in the left hemisphere contributes to clinical and cognitive deterioration in multiple sclerosis: a 5-year study. Hum Brain Mapp. 2017;38:5648–65.
53. Seghier ML. Laterality index in functional MRI: methodological issues. Magn Reson Imaging. 2008;26:594–601.